**ORIGINAL ARTICLE**

# Examination of electrochemical machining parameters for AA6082/ZrSiO$_4$/SiC composite using Taguchi-ANN approach

K. Srividya[1] · S. Ravichandran[2] · M. Thirunavukkarasu[3] · Itha Veeranjaneyulu[4] · P. Satishkumar[5] ·
K. Bharadwaja[6] · N. Srinivasa Rao[7] · Ram Subbiah[8] · Javvadi Eswara Manikanta[7]

**Abstract**

Aluminum alloy is a widely utilized material in the modern automotive industry due to its lightweight properties and corrosion resistance. Unconventional machining processes, particularly electrochemical machining (ECM) offer effective means to work with such materials. This study focuses on assessing the influence of four specific parameter combinations on the machining of AA6082/ZrSiO$_4$/SiC alloy. This work also analyzes the impact of critical ECM process parameters, including tool feed rate, applied voltage, electrolytic concentration, and electrode type on the output response variables. These variables encompass characteristics such as material removal rate (MRR) and surface roughness (SR), and their relationships are explored through the application of the Taguchi design of experiments methodology. The analyzed experimental data were employed to train an Artificial Neural Network (ANN) model aimed at achieving more accurate predictions to increase the MRR and reduce SR. The ANN setup is a multilayer perceptron utilizing a feed forward architecture, denoted as (4–20–2). This notation indicates that there are 4 nodes in the input layer, twenty neurons in the hidden layers, and 2 nodes in the output layer. The ANN predictions yield an R$^2$ value of 0.98003 and MSE within the range of 0.02413, specifically for the experiment dataset. The results of the regression study strongly indicate that the ANN model can effectively and reliably predict both MRR and SR with a high degree of precision. The scanning electron microscope (SEM) micrograph of the surface also indicates an improved surface finish with brass tool as compared to graphite.

**Keywords** ANN · Optimization · ECM process · Al alloy · MRR and SR

✉ Ram Subbiah
Ram4msrm1@gmail.com

K. Srividya
srividya@pvpsiddhartha.ac.in

S. Ravichandran
pveearr@gmail.com

M. Thirunavukkarasu
er_arasu@yahoo.co.in

Itha Veeranjaneyulu
anjimech@gmail.com

P. Satishkumar
p.sathishkumar10@gmail.com

K. Bharadwaja
bharadwajak2007@gmail.com

N. Srinivasa Rao
srinivasaraon@svecw.edu.in

Javvadi Eswara Manikanta
manijem66@gmail.com

[1] Department of Mechanical Engineering, P V P Siddhartha Institute of Technology, Kanuru, Vijayawada 520007, India

[2] Department of Mechanical Engineering, KIT-Kalaignar Karunanidhi Institute of Technology, Coimbatore, India

[3] Department of Automobile Engineering, Dr.Mahalingam College of Engineering and Technology, Pollachi, Tamilnadu, India

[4] Department of Mechanical Engineering, Aditya Engineering College, Surampalem, India

[5] Department of Mechanical Engineering, Rathinam Technical Campus, Coimbatore, Tamil Nadu, India

[6] Department of Mechanical Engineering, Malla Reddy Engineering College (A), Secunderabad, India

[7] Department of Mechanical Engineering, Shri Vishnu Engineering College for Women (A), Bhimavaram 534202, India

[8] Department of Mechanical Engineering, Gokaraju Rangaraju Institute of Engineering and Technology, Hyderabad, India

# 1 Introduction

The superlative non-traditional production process in the industrial sector is electrochemical machining (ECM). With the support of an electrolyte solution, electrical current is transmitted across the cathode end tool and anode workpiece. It operates according to Faraday's Law of Electrolysis [1]. Superalloy materials are being machined using an electrochemical method into the required design shapes [2].The metal ions of the anode combine with the hydroxyl ions released at the cathode during the electrolysis process to form a metal hydroxide. As a result, the metal is precipitated in an electrolytic cell and removed as sludge. This procedure continues until the work item takes on the shape that the tool has produced in it [3]. In the medical field, implant materials such as titanium alloy and aluminium alloy specimens should have the best possible surface quality [4, 5]. Hasan Demirtas et al. aimed to enhance the surface quality of-TiAl AM parts created using the EBM technique. By adjusting the electrolyte type, pulse rate, and feed rate, among other key variables, the specimens were machined by ECM, and the impacts of these changes on the surface characteristics were analyzed. The Ra values were discovered to have fallen from 26.73 to 2.47 m in the scan direction and from 35.39 to 3.25 m in the build direction. For both directions, the surface irregularity is reduced by about 91% [6]. Numerous computational intelligence techniques have been used to solve optimization problems. To handle problems involving Multi-Objective Optimization, the PSO with combined normalized objective is introduced. Selecting the correct values for electrolytic machining process parameters is crucial for optimizing the process performance parameter [7]. T.A. Selvan et al. explored the surface finish and material extraction features of Inconel 718 super-alloy. The experiment was carried out utilizing a titanium tool and electrochemical machining with various variables. The optimum strategy was done based on Taguchi's related grey relational technique using Minitab 19 software [8]. In order to build effective strategies for multi-material systems, Shatarupa Biswas et al. developed the GA/PSO combined MOMLN for multi-material optimization for finding the ideal parameters for machining of IN625/718 and noted that GA combined model's accuracy is marginally greater than the PSO [9]. The optimal parametric configuration is identified using GRA, TOPSIS, and PSI to analyze the MRR, TWR, and SR for machining Inconel 71. ANOVA is used to statistically analyze the experimental data, and the contribution level of each parameter is given in order to provide the best results [10]. The influence of WEDM process factors on the tapered workpiece manufactured of the AA5454 alloy was investigated. This method is used to make slots in a tapered angle of 30°, 45°, and 60° on the workpiece along with variables peak

discharge current, and pulse-off time [11]. In order to determine optimal parameters for the desired variables, regression models and GA are performed [12]. ANN are used in a multi-variable optimization process to choose the most practical pulse width, timing, wire winding velocity, and wire tension for stainless steel to achieve the ideal SR. Huang and Liau et al. [13] investigated the effects of feed rate, pulse timing, wire tension, and flushing pressure on the MRR and SR of the SKD-11. The MRR was found to be significantly impacted by the table feed rate, whereas SR was mostly influenced by pulse-on time. Rajurkar et al. [14] talked about increasing accuracy by employing passive electrolytes to reduce sludge. The waste generated from the machining surface had a minimal machining allowance to increase the localization impact and the effectiveness of the ECM process. sodium nitrate has been used to enhance machining features including machining precision. Kozak and Rajurkar researched pulse electrochemical micromachining for micro components on a cutting surface which are stress-, burr-, and crack-free. Process variables which include applied voltage and feed rate have been studied for their effects on performance measures. The inter-electrode gap is minimized to promote localized dissolution and raise accuracy in the ECM process [15, 16].

The link between the efficiency of current and current density was the main topic of Lin Tang et al.'s study [17]. An analysis was conducted on the impact of current density on grain boundary corrosion, machining velocity, and surface roughness. The findings demonstrated that, at various concentrations, the NaCl electrolyte's current efficiency was 100%. The 10 percent NaCl electrolyte can achieve 3.6 mm/min cathode feed speed, Ra 0.08 µm surface roughness, and 411.4 $mm^3$/min material removal rate at 24 V voltage, 30 °C electrolyte, and 0.8 MPa electrolyte pressure. subsequently examined forward flow to forward flow with additional backpressure, they discovered that in the NaCl electrolyte, the surface roughness value dropped dramatically at 3.6 mm/min. Shirish D. Dhobe et al. [18] presented an experimental examination of the surface properties obtained on titanium using electrochemical machining. Experiments have effectively investigated the effects of applied voltage between the tool and workpiece, as well as electrolyte flow velocity during the ECM process, on the creation of various surface characteristics. An attempt has been made to create a surface and a self-generated oxide layer, which will help titanium implants in biomedical applications withstand corrosion and chemicals better. The oxide-layered machined surface's surface roughness was found to be between 3.09 and 3.66 µm, which is within the region where an implant and bone can functionally bond.

This research is to assess the impact of a comprehensive set of parameters in the ECM process when machining the AA6082/ZrSiO$_4$/SiC alloy. This investigation involves the
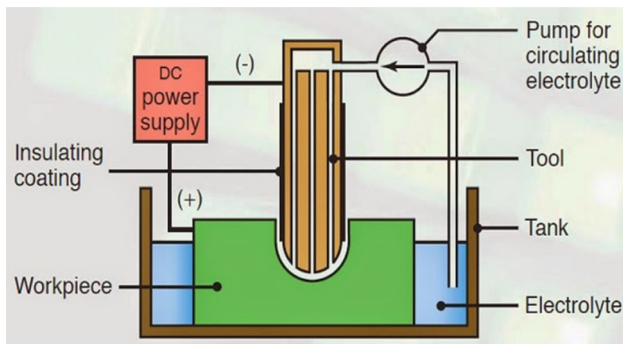
**Fig. 1** ECM setup

**Table 1** ECM parameters

| Parameters | Level 1 | Level 2 | Level 3 |
|---|---|---|---|
| Tool feed rate | 0.20 | 0.30 | 0.40 |
| Applied voltage | 25 | 35 | 45 |
| Electrolyte concentration | 30 | 40 | 50 |
| Electrode Type | Copper (1) | Brass (2) | Graphite (3) |

measurement of several output parameters, including material removal rate and surface roughness, while systematically altering input parameters such as tool feed rate, applied voltage, electrolyte concentration, and electrode types. Furthermore, microstructural analysis has been conducted to elucidate grain variations around the machined region of each specimen, and optimal parameters have been determined through the utilization of Minitab statistical software An Artificial Neural Network (ANN) is employed to construct a prediction model using the LMA with MATLAB-2016a version. This model is based on a FFBN network and is designed to analyze MRR and SR. AA6082/ZrSiO4/SiC finds common use in the automotive sector, where it is employed in the production of various components like body panels, wheels, and chassis structures. The alloy's advantageous blend of strength and lightweight characteristics plays a crucial role in enhancing overall fuel efficiency.

## 2 Materials and methods

According to Fig. 1, ECM setup contains of a power source, a control unit for setting process parameters, a system for supplying electrolyte, the tool and the work piece [19]. Due to its significance in manufacturing industries, AA6082/ZrSiO4/SiC alloy with a dimension of (60 mm* 60 mm *5 mm) was designated as a workpiece which is secured using plastic clamps to prevent uneven calibration, and acrylic tank is locked to prevent electrolyte leakage. Using the screw mechanism, the cathode is manually positioned as close to the anode as feasible without coming into touch. After adding enough electrolyte to the machining chamber to completely submerge the area between the tool and workpiece, the ECM process begin. The tool is sunk in order to complete this operation. In the current study, machining tests were carried out using various ECM parameter combinations using a Taguchi-based L9. The L9 orthogonal array enables a methodical and effective exploration of the experimental design space. It furnishes a well-balanced

and representative collection of experiments, aiding in the identification of the most impactful factors influencing the process while keeping the number of experimental runs relatively small. the selected parameter's levels and chemical elements of AA6082 are shown in Tables 1 and 2 respectively. AA 6082 possesses tensile strength of 260 MPa, yield strength of 236 MPa and elongation of 7–10%. The selection of parameters in electrochemical machining (ECM) is crucial for achieving the desired material removal rate, surface finish, and dimensional accuracy. The criteria for parameter selection in ECM include considerations related to the material being machined, the desired outcome, and the specific constraints of the machining process. Finding the optimal set of parameters often involves a combination of theoretical understanding, empirical testing, and continuous refinement based on feedback from the machining process.

In each of the trail conditions and for every replication the MRR and SR are measured. The machining for each trail is carried out for 5 to 10 min. Taguchi suggests the use of the S/N ratio which measure the excellence features conflicting from the chosen values. The quality characteristics for MRR is engaged as "higher is better" and for SR "lower is better". To identify the surface generation parameters that are statistically significant, an ANOVA is performed. The optimal grouping of the surface generation-based process parameters is forecasted with the S/N and ANOVA analysis. MRR was measured by electronic balance during machining. The measured weight is then converted into a volumetric material removal rate as it is generally measured in mm$^3$/min. The volumetric MRR is found by applying the following formula:

$$MRR = (\text{Reduction in weight}) / (\text{density of the alloy} \times \text{machining time})$$

Surface roughness is linked to the arithmetic average deviance of a surface peak and valley which are expressed in micro-meters ($\mu$m). The SR is measured by Mitutoyo surftest, having a range of 0.01–200 $\mu$m.

| Table 2 Chemical composition-AA6082 | Mn | Fe | Mg | Si | Zn | Cu | Cr | Ti | Al |
|---|---|---|---|---|---|---|---|---|---|
| | 0.65 | 0.4 | 1.1 | 1.2 | 0.2 | 0.10 | 0.15 | 0.05 | Bal |
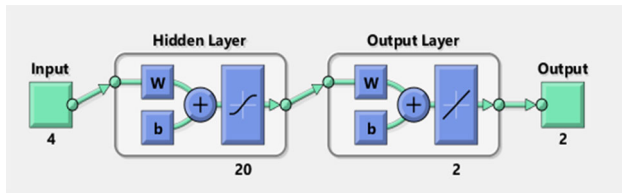


**Fig. 2** ANN structure

## 3 Artificial neural network

An artificial neural network (ANN) is a mathematical model that autonomously approximates the functioning of traditional neural systems. In this study, a multilayer perceptron (MLP) was created, consisting of four input neurons representing tool feed rate, applied voltage, electrolytic concentration, and electrode type. These inputs were connected to hidden layers of neurons, while two output neurons represented the MRR and SR. In the pursuit of enhancing prediction accuracy using experimental data, an iterative approach was employed to ascertain the optimal number of neurons in the hidden layer. It was deduced that, to construct a proficient model tailored to the given dataset, a minimum of twenty neurons in the hidden layer was imperative. Nonetheless, increasing the number of neurons posed a potential risk of overfitting the model. The final model was constructed using 90% of the experimental data for training purposes, with the enduring data being separated between model validation and testing [20]. The process of solving fitting issues involved training the neural network to establish relationships between input variables and a set of numerical targets, as depicted in Fig. 2.

## 4 Result and discussion

### 4.1 The influence of parameters on MRR

The contour plot serves as a visual representation that effectively depicts the behavior of a two-dimensional function within a specified domain of interest. This tool proves valuable for gaining insights into how a function responds to variations in two input parameters, particularly concerning its output response such as MRR. In Fig. 3a–f, a series of contour plots is presented, illustrating the relationship between input parameters and MRR. Notably, Fig. 3a reveals that maintaining a tool feed rate of 0.4 mm/min and an applied voltage of

25 V tends to increase MRR. Additionally, a slight further increase in MRR is observed when the applied voltage is raised to 35 V. Moving to Fig. 3b, it portrays a contour plot depicting the interplay between tool feed rate and electrolyte concentration. Here, we observe that the MRR tends to rise when maintaining an electrolyte concentration of 40 g/liter and a tool feed rate of 0.35 mm/min. This phenomenon can be attributed to the fact that higher electrolyte concentrations enhance conductivity, consequently increasing stray currents. This, in turn, diminishes localization effects, ultimately leading to a reduction in MRR [21]. Figure 3c illustrates a plot that depicts the connection between the tool feed rate and the type of electrode used. Notably, it becomes evident that maintaining a brass electrode tends to increase the MRR. The machined surface quality is influenced by the tool feed rate. An elevated feed rate can result in rougher surfaces due to heightened tool engagement with the workpiece. Conversely, lower feed rates may produce smoother surfaces, although there is a trade-off as it could lead to a reduction in Material Removal Rate (MRR). The type of electrode contributes to determining the ultimate surface finish. The composition and state of the electrode can impact the electrochemical reactions occurring at the tool-workpiece interface, thereby influencing the quality of the machined surface. Choosing the right electrode is crucial to attaining the intended surface finish. As shown in Fig. 3d, when exploring the influence of the parameters on MRR, applied voltage emerges as the most dominant factor. This is particularly evident when considering the combination of electrolyte concentration. When higher voltage is applied, it results in a decrease in stray current and side current, ultimately leading to a reduction in MRR [22]. Figure 3e and f depict plots that explore the relationship between applied voltage and electrode type, as well as electrolyte concentration and electrode type, respectively. These graphical representations provide valuable insights. From these plots, it becomes evident that when an electrolyte concentration of 40 g/l is maintained in conjunction with a brass electrode, there is a notable increase in the MRR for the aluminum alloy workpiece.

### 4.2 The influence of parameters on SR

In Fig. 4a–f, a set of contour plots is presented to illustrate the correlation between input parameters and Surface Roughness (SR). Figure 4a indicates that keeping the tool feed rate at 0.2 mm/min and applying a voltage of 35 V results in a
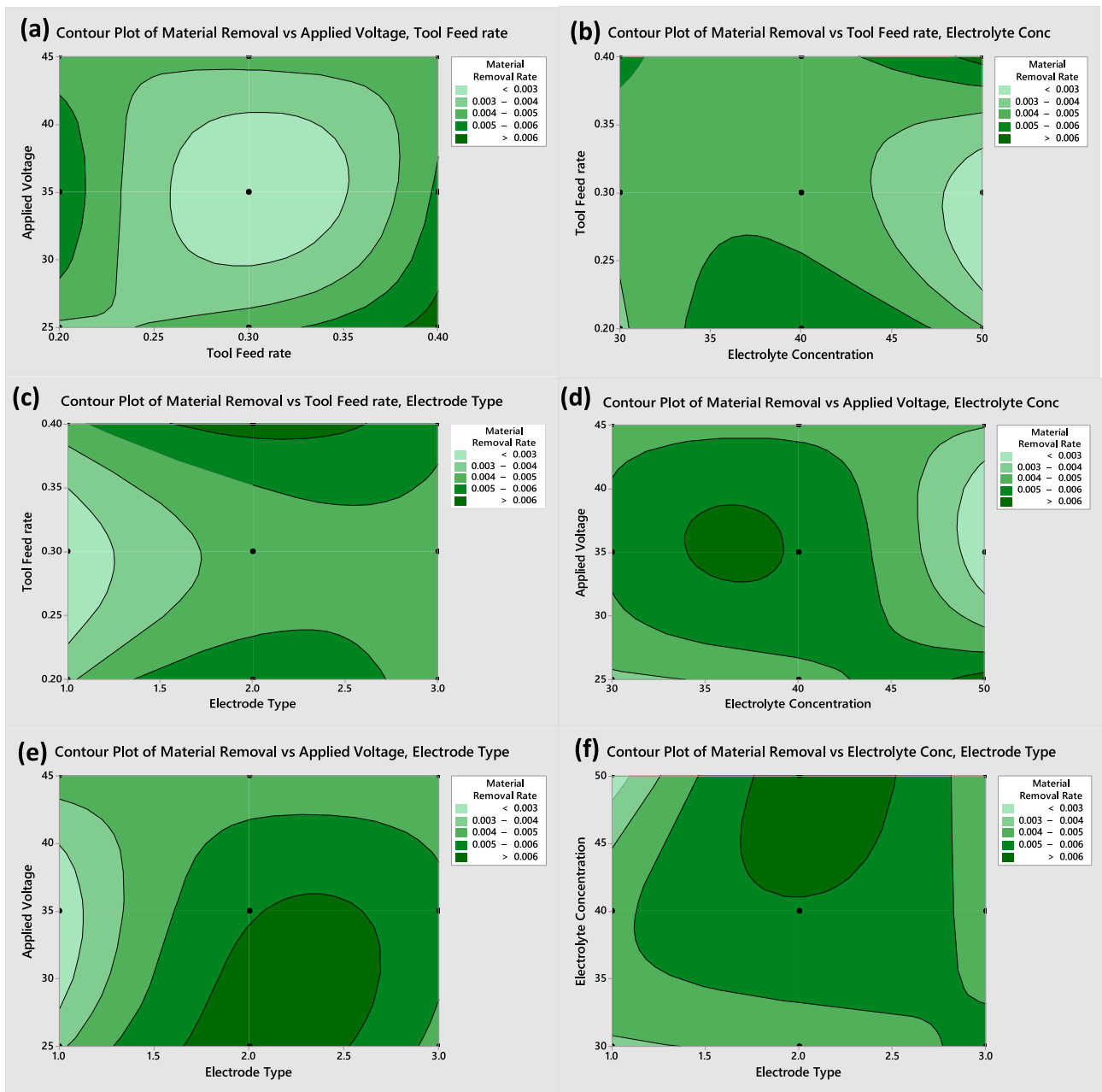
**Fig. 3** contour plots for MRR

reduction in SR. Moving on to Fig. 4b, it reveals the interplay between the tool feed rate & electrolyte concentration. It is noticeable that maintaining an electrolyte concentration of 40 g/l and feed rate of 0.4 mm/min tends to increase the SR. Figure 4c showcases a plot illustrating the connection between the tool feed rate and the type of electrode. it becomes evident that using a copper electrode leads to an elevation in SR. In Fig. 4d, it is observed the relationship between voltage and electrolyte concentration. When a higher voltage is applied, it increases in current, ultimately leading to higher surface roughness. Figure 4e and f depict

plots exploring the connection between applied voltage and electrode type, as well as electrolyte concentration and electrode type, respectively, to surface roughness. These plots highlight that maintaining a copper electrode alongside an increase in voltage results in elevated surface roughness. The experiment results reveal that the highest MRR value was achieved in experiment number 7, while the lowest MRR value was observed in experiment number 5. Experiment 7 utilized a parameter combination of TF at 0.4 mm/min, AV at 25 V, EC at 50 g/l, and ET at 2. Conversely, experiment 5 employed a parameter combination of TF at 0.3 mm/min, AV
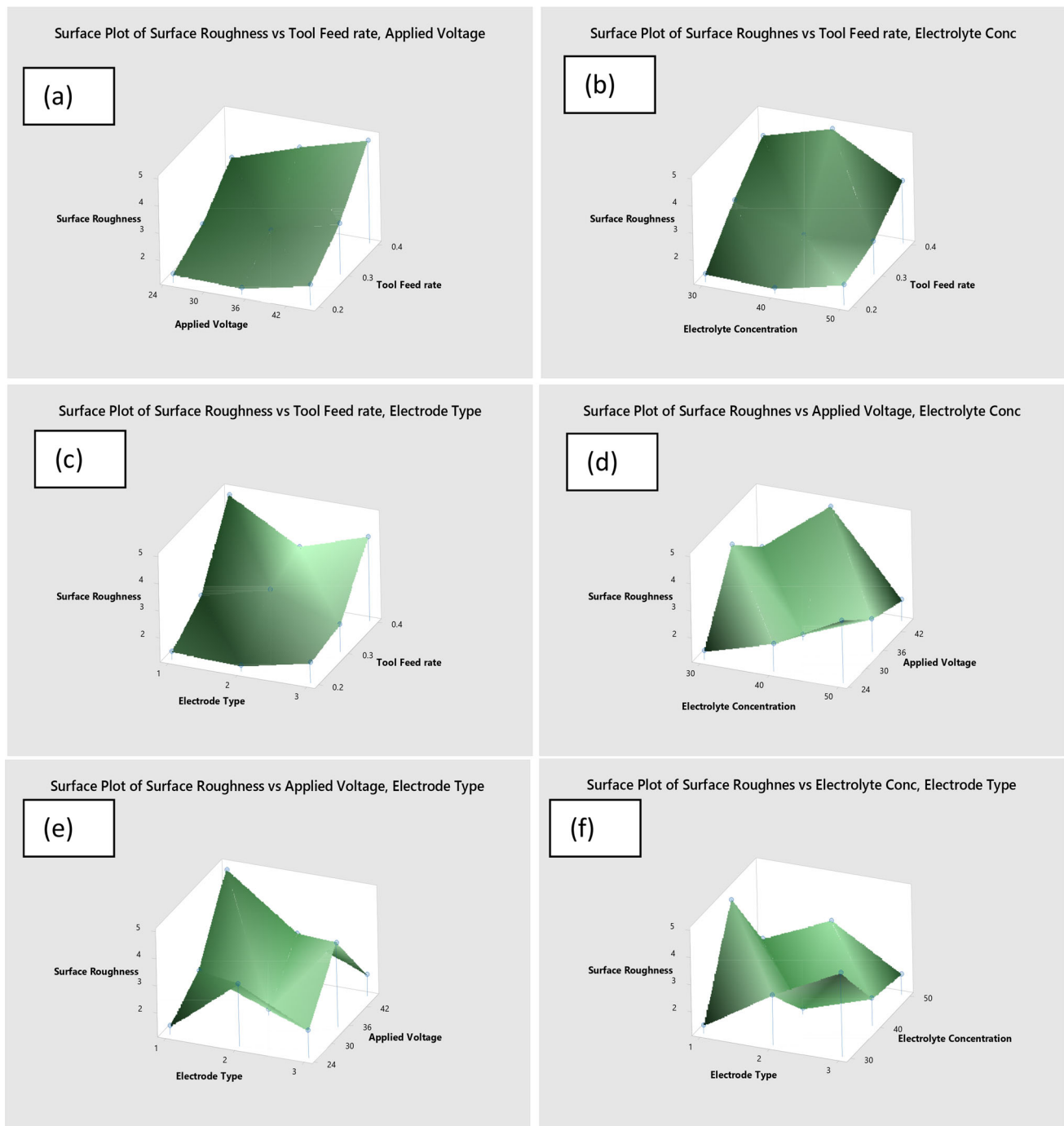
**Fig. 4** contour plots for SR

at 35 V, EC at 50 g/l, and ET at 1. These findings indicate that, based on the MRR results, the use of a brass electrode, Tool Feed rate increment and a reduction in the Applied Voltage all contribute to the enhancement of MRR values. Figure 5a and b display the means and SN ratio plot pertaining to MRR. These figures offer insight into the influence of various ECM parameters on determining the optimal MRR value. Based

on the Table 3, it has been determined that the most favorable parameter combination for achieving optimal MRR is TF3-AV1-EC2-ET2.Notably, the utilization of a brass electrode during alloy machining, while keeping key parameters constant (tool feed rate at $-0.4$ mm/min, applied voltage at 25 V, and electrolyte concentration at 40 g/liter), leads to an increase in MRR. The thermophysical properties of the electrode material play a pivotal role in determining its
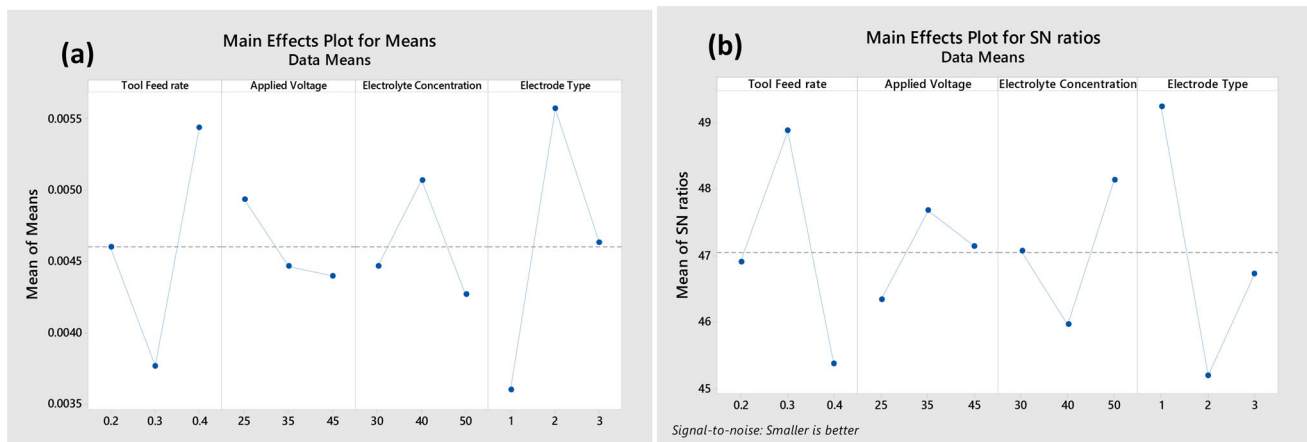
**Fig. 5** Means and SN ratio plot for MRR

**Table 3** MRR and SR results

| S. no. | Tool feed rate (TF) (mm/min) | Applied voltage (AV) (V) | Electrolyte concentration (EC) (g/l) | Electrode type (ET) | MRR (mg/min) | SR (μm) |
|---|---|---|---|---|---|---|
| 1 | 0.2 | 25 | 30 | 1 | 0.0038 | 1.41 |
| 2 | 0.2 | 35 | 40 | 2 | 0.0059 | 1.31 |
| 3 | 0.2 | 45 | 50 | 3 | 0.0041 | 1.86 |
| 4 | 0.3 | 25 | 40 | 3 | 0.0046 | 2.1 |
| 5 | 0.3 | 35 | 50 | 1 | 0.0023 | 2.3 |
| 6 | 0.3 | 45 | 30 | 2 | 0.0044 | 1.96 |
| 7 | 0.4 | 25 | 50 | 2 | 0.0064 | 2.39 |
| 8 | 0.4 | 35 | 30 | 3 | 0.0052 | 3.19 |
| 9 | 0.4 | 45 | 40 | 1 | 0.0047 | 2.88 |

ability to efficiently process energy during machining and facilitate material removal from the aluminum alloy workpiece. It is crucial to ionize the gap between the electrode and workpiece to enable the discharge of current and the generation of robust sparks, which significantly affect MRR. In the case of a brass electrode, a considerably higher tool feed rate is required to release electrons into the gap compared to both copper and graphite electrodes (Table 4). On the other hand, the graphite electrode, with its carbon-based composition, necessitates lower temperatures to emit electrons, and it doesn't demand an extended time frame to establish the necessary energy channel for enhancing MRR. Table 5 displays the ANOVA results for MRR, clearly demonstrating that the most significant factor in MRR is the type of electrode (47.08%), followed by the tool feed rate and other related parameters. This analysis underscores the significant impact of machining variables on MRR, while it is worth noting that the material strength used has a minimal effect on MRR.

The experimental results highlight that the highest surface roughness value was attained in experiment number 8, while the lowest surface roughness was observed in experiment number 2. Experiment 8 employed a parameter combination of TF (Tool Feed) at 0.4 mm/min, AV (Applied Voltage) at 35 V, EC (Electrolyte Concentration) at 30 g/l, and ET (Electrode Type) at 3. Conversely, experiment 2 utilized a parameter combination of TF at 0.2 mm/min, AV at 35 V, EC at 40 g/l, and ET at 2. These findings suggest that, in terms of SR results, employing a brass electrode, decreasing the Tool Feed rate, and increasing the Applied Voltage all contribute to reducing SR, resulting in an improved surface finish for the alloy workpiece.

Figure 6a and b present the means and signal-to-noise ratio (SN ratio) plots related to surface roughness. These figures provide insights into the impact of various Electrochemical Machining (ECM) parameters on achieving the optimal SR value. Based on the Table 6, it has been determined that the most favorable parameter combination for achieving optimal SR is TF1-AV1-EC2-ET2. Notably, when machining alloy with a brass electrode, while keeping key parameters constant (tool feed rate at 0.2 mm/min, applied voltage at 25 V,

**Table 4** SN ratio for MRR

| Level | Tool feed rate | Applied voltage | Electrolyte concentration | Electrode type |
|---|---|---|---|---|
| 1 | 46.91 | 46.34 | 47.07 | 49.24 |
| 2 | 48.88 | 47.68 | 45.96 | 45.20 |
| 3 | 45.37 | 47.14 | 48.13 | 46.72 |
| Delta | 3.51 | 1.33 | 2.17 | 4.05 |
| Rank | 2 | 4 | 3 | 1 |

**Table 5** ANOVA for MRR

| Source | DF | SS | MS | F | P | % |
|---|---|---|---|---|---|---|
| Tool feed rate | 2 | 18.5619 | 9.2810 | 2.92 | 0.000 | 34.67 |
| Applied voltage | 2 | 2.7070 | 1.3535 | 0.389 | 0.004 | 5.06 |
| Electrolyte concentration | 2 | 7.0438 | 3.5219 | 0.958 | 0.003 | 13.19 |
| Electrode type | 2 | 25.0465 | 12.5233 | 3.62 | 0.000 | 47.08 |
| Residual error | 0 | 0 | 0 | | | |
| Total | 8 | 53.3592 | | | | |
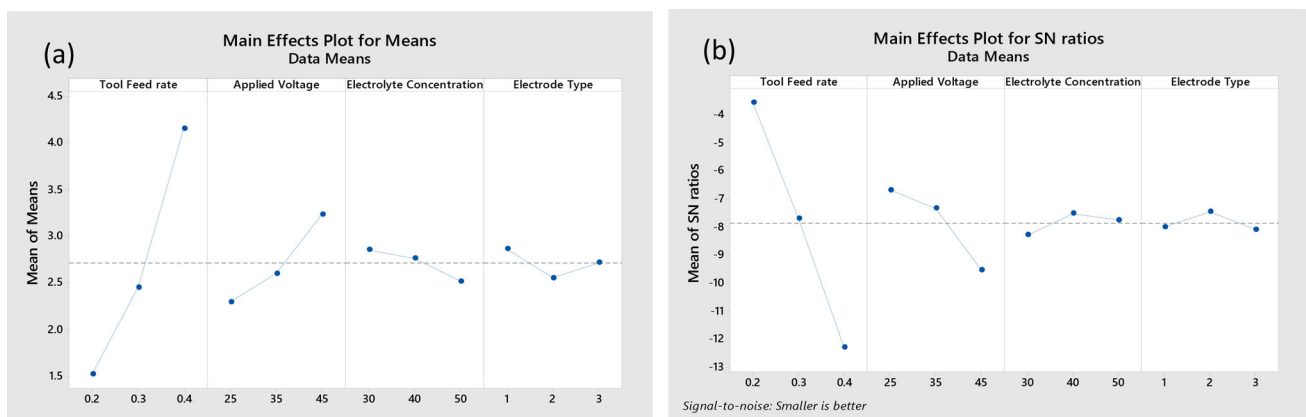


**Fig. 6** Means and SN ratio plot for SR

and electrolyte concentration at 40 g/liter), there is a reduction in SR. It is essential to ionize the space between the electrode and workpiece to facilitate current discharge and the generation of robust sparks, both of which significantly affect SR. Table 7 displays the ANOVA results for surface roughness, clearly illustrating that the significant parameter affecting SR is the tool feed rate (88.33%), followed by the applied voltage and other related parameters. This analysis emphasizes the substantial impact of machining variables on SR. It is worth noting that the material strength used has a minimal effect on SR.

## 4.3 SEM analysis

SEM may be used to analyze the shape and structure of ($ZrSiO_4$ and SiC) nanoparticles. The distribution and form of

**Table 6** SN ratio for SR

| Level | Tool feed rate | Applied voltage | Electrolyte concentration | Electrode type |
|---|---|---|---|---|
| 1 | − 3.573 | − 6.678 | − 8.285 | − 7.996 |
| 2 | − 7.702 | − 7.341 | − 7.519 | − 7.458 |
| 3 | − 12.272 | − 9.528 | − 7.743 | − 8.093 |
| Delta | 8.699 | 2.851 | 0.765 | 0.635 |
| Rank | 1 | 2 | 3 | 4 |

**Table 7** ANOVA for SR

| Source | DF | SS | MS | F | P | % |
|---|---|---|---|---|---|---|
| Tool feed rate | 2 | 113.603 | 56.80 | 20.23 | 0.000 | 88.33 |
| Applied voltage | 2 | 13.348 | 6.67 | 2.56 | 0.0045 | 10.38 |
| Electrolyte concentration | 2 | 0.930 | 0.46 | 0.135 | 0.068 | 0.73 |
| Electrode type | 2 | 0.701 | 0.35 | 0.128 | 0.076 | 0.71 |
| Residual error | 0 | 0 | 0 | | | |
| Total | 8 | 128.582 | | | | |

the two types of nanoparticle materials are shown in Fig. 7a and b respectively. These figures demonstrate how certain $ZrSiO_4$ and SiC particles have combined. Both types of nanoparticles included agglomerated and small rounded particles, as well as spherical and irregularly shaped particles. Van-der-Waal forces between each of the particles may be connected to the tendency for particle agglomeration [23].

The SEM micrographs are mentioned for MRR by using brass and graphite electrode in Fig. 8a and b. The electrochemical reactions in ECM generate heat in the machining zone. A higher tool feed rate helps in dissipating this heat more effectively. It prevents localized overheating, which can negatively affect the machining process by leading to the formation of passive layers or other undesirable reactions. Effective heat dissipation maintains stable machining conditions and contributes to an increased MRR. Brass electrode is an excellent electrical conductor, which is a crucial property for ECM. During ECM, an electric current passes between the workpiece and the electrode, causing electrochemical reactions. The high electrical conductivity of brass ensures efficient current flow and, consequently, higher MRR and the graphite electrode indicate particle deposition, globules, and white layer. The increase in layer with depositions, pockmarks, and white layer thickness can be seen on the surface machined with a graphite electrode due to an increase in carbon element with graphite electrode and also cracking of dielectric fluid and material deposition from electrode material.

Surface roughness of Al alloy workpiece for both brass and graphite electrode is shown in Fig. 9a and b. The improvement in surface finish machined with the brass electrode as evaluated against graphite electrode is also seen from SEM micrograph Fig. 9a. The scientific reasons for using a brass electrode to expand surface finish in ECM include its erosion characteristics, control over material removal, dampening of electromechanical effects, generation of fine wear debris for polishing, compatibility with electrolytes, and reduced risk of passivation. These properties collectively contribute to achieving a high-quality surface finish in ECM applications.

## 4.4 Prediction of MRR and SR using ANN-LM model

MATLAB R2016a was employed to predict the MRR and SR. The experimental data served as the fundamental source of input–output information for training the neural network. This dataset was subsequently divided into two matrices: one for inputs and another for outputs. Various network configurations were explored, incorporating different training algorithms, and adjustments were made to identify the optimal architecture. The experimental dataset, consisting of nine sets of data, was randomly partitioned into three segments using the MATLAB R2016a neural network toolbox, allocating 70% for training, 15% for testing, and 15% for validation, respectively [24, 25]. This division involved using seven data sets for training, one for testing, and one for validation, a strategy aimed at preventing the network from overfitting [26]. For this particular dataset, the Multilayer Perceptron (MLP) network was chosen, employing the Tangential–Sigmoid function for the hidden layer, a linear transfer function on the output layer, and the LM Algorithm. Neural network training uses the Levenberg–Marquardt (LM) algorithm. It's a numerical optimization technique that blends elements of the Gauss–Newton method and gradient descent. when standard gradient descent techniques might converge slowly, the LM algorithm is frequently employed [27–29]. This choice was made due to the algorithm's speed and its minimal memory requirements when compared to other algorithms [30].

The optimal conformation for the ANN model was determined to be a 4–12–2 network structure, indicating input layer (4 nodes), hidden layer (12 nodes), and output layer (2 nodes). To evaluate the regression fit and the overall performance of the developed model, we employed two key parameters, namely $R^2$ (coefficient of determination) and MSE (mean squared error) [31–37]. The precision of the ANN model was evaluated across training, validation, and testing datasets to gauge its effectiveness, employing $R^2$ and MSE metrics [33, 38–43]. The resultant values are mentioned in Table 8. The regression work was employed to inspect the relationship between the inputs/outputs generated by ANN and their corresponding target values [44–48]. The preferred ANN architecture, denoted as (4–12–2), is depicted in the comprehensive regression graph presented in Fig. 8. Notably,
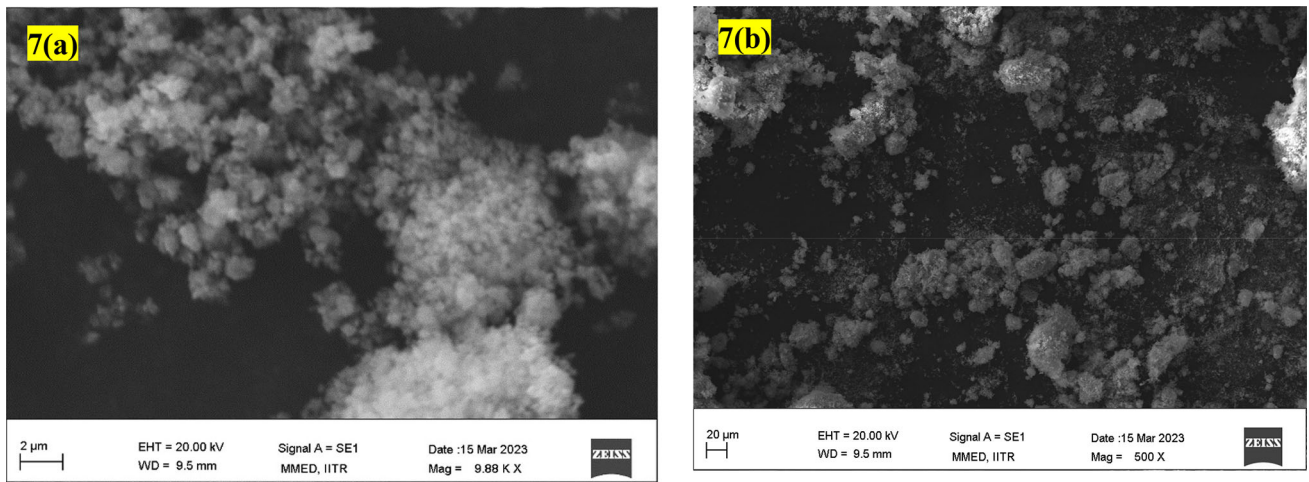
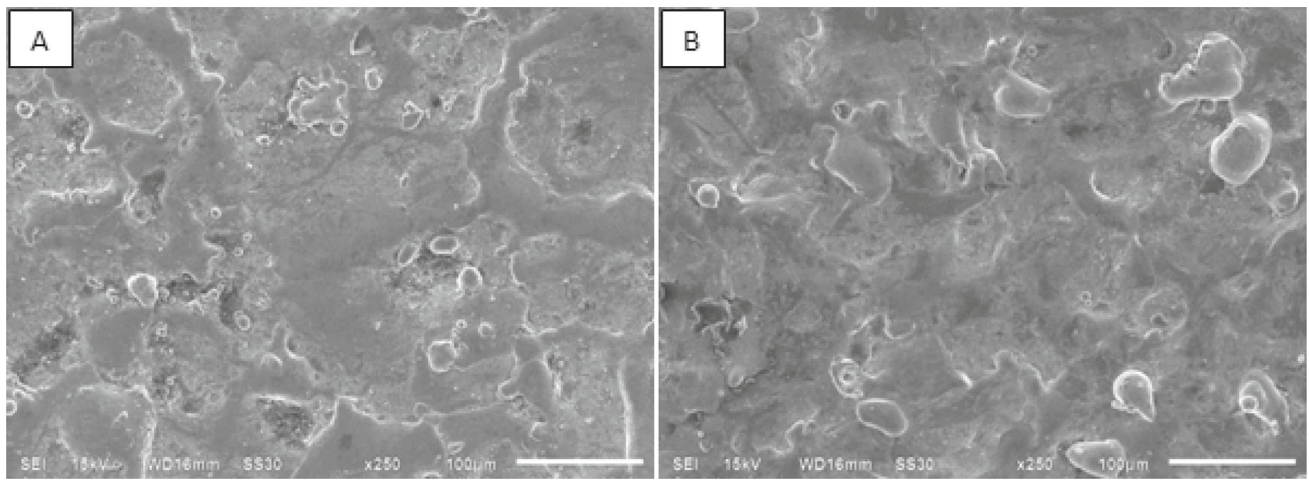**Fig. 7** SEM images for **a** ZrSiO$_4$ nano particles **b** SiC nano particles



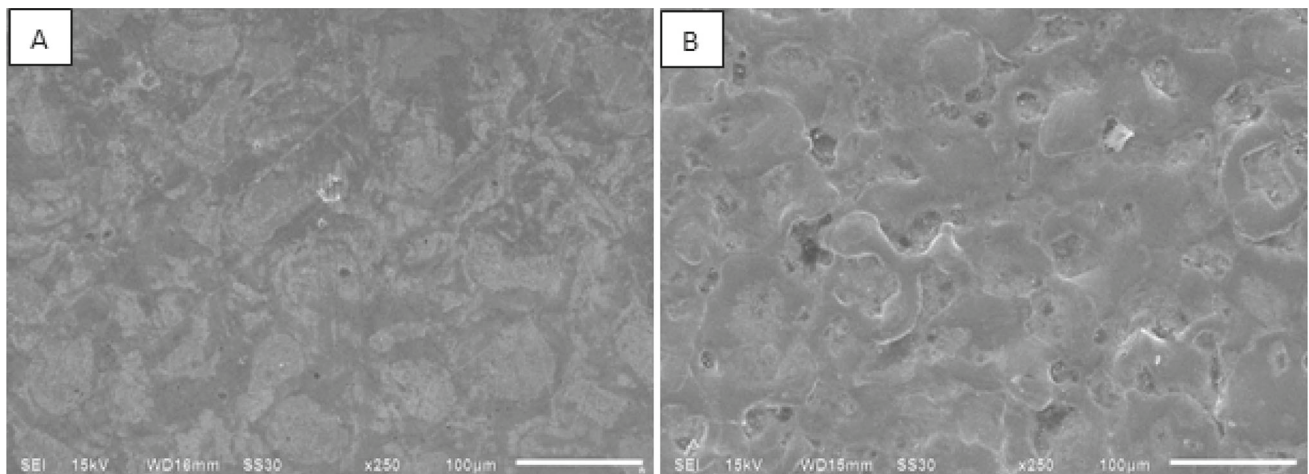**Fig. 8** SEM micrographs for MRR **A** Copper electrode **B** Graphite electrode



**Fig. 9** SEM micrographs for SR **A** Copper electrode **B** Graphite electrode

**Table 8** Performance evaluation for 4–12–2 ANN model

| Data set | R | MSE |
|---|---|---|
| Train | 0.99846 | 0.05347 |
| Validation | 1 | 0.07102 |
| Test | 1 | 0.05638 |

the detected correlation coefficients for the training, validation, and testing sets are 0.99846, 1, and 1, respectively. When considering all datasets encompassing training, validation, and testing, the correlation coefficient is determined to be 0.98003. The provided information encompasses regression diagrams for the ANN, covering a range of neurons from 1 to 20. These charts reveal an $R^2$ value of 0.98003, indicating that the fit accounts for 98.003% of the overall variation in the average data. Essentially, this demonstrates a high degree of concordance between the experimental outcomes [49]. Figure 10 displays scatter plots comparing predicted values to actual values across various data sets, including training, validation, testing, and the complete dataset. Figure 11 illustrates an error histogram, quantifying the disparity between predicted values and targeted values. The histogram is divided into bins, representing different ranges of error [50–52].

The Y-axis denotes the samples number from the dataset falling to each bin [53–55]. The bin's height for the training
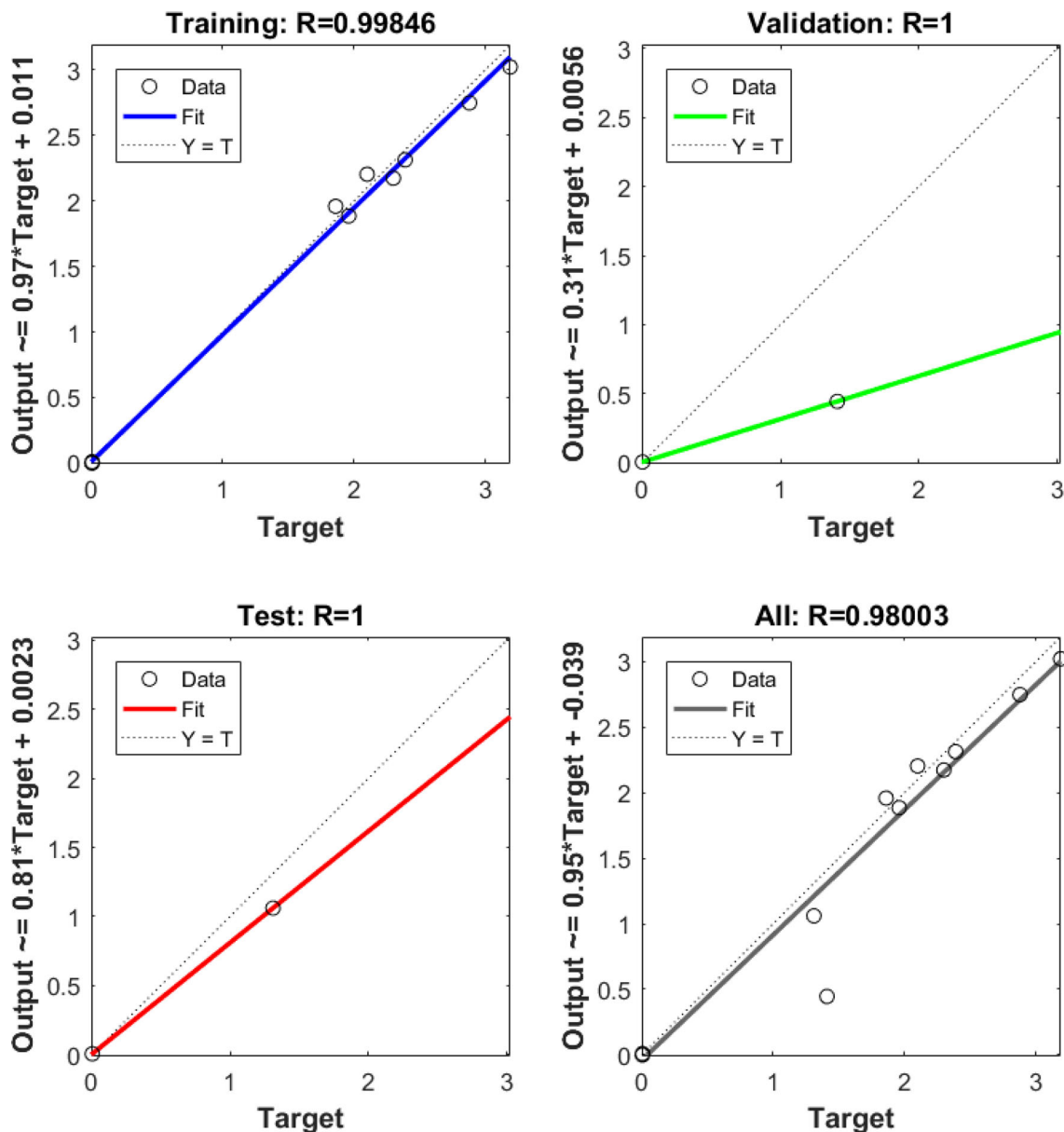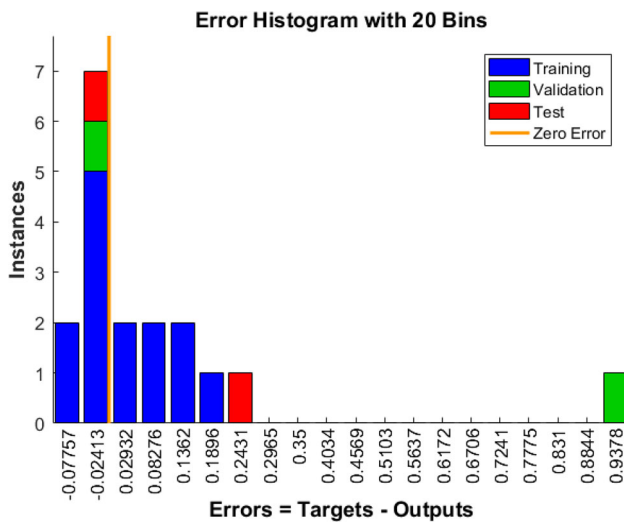


**Fig. 10** Regression Fit in ANN

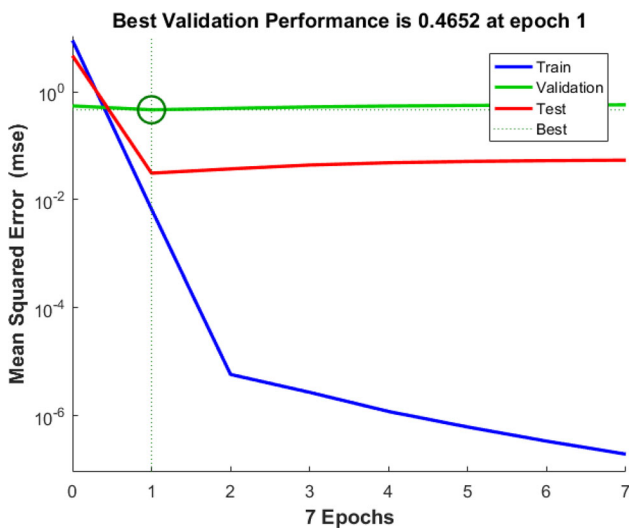**Fig. 11** Error histogram



**Fig. 12** Validation performance diagram

set is around 2, and for the validation dataset which close to this value. This suggests that the majority of samples exhibit an error of 0.02413.

The zero-error line is positioned slightly to left of the center bin and also has an error 0.02413. For predicting the MRR and SR, the most optimal validation was achieved at epoch 1, as shown in Fig. 12, where the MSE graph displays results from 7 epochs of all datasets. In general, as the number of training epochs increases, the error tends to decrease. However, it's worth noting that once the network starts overfitting the training data, the validation dataset error may begin to rise [56–58]. This result confirmed the model's capability, demonstrating that the experimental result closely matched the prediction made by the ANN with a relative discrepancy of less than 1. This indicates that the ANN-derived model

effectively captures the connection among the input variables and the outputs. The findings also underscore a significant alignment between the neural system's predictive capabilities and established testing validation standards.

## 5 Conclusion

- In this current investigation, we have undertaken an effort to discover the impact of various process parameters employed in the ECM process when machining Aluminium alloy (AA6082 /ZrSiO$_4$ /SiC) to achieve improved performance metrics related to Material Removal Rate (MRR) and surface roughness (SR). Based on the outcomes of our experiments, the following findings have been derived.

- The investigation revealed that the most advantageous combination of parameters for achieving the highest MRR is TF3-AV1-EC2-ET2. Importantly, employing a brass electrode in the machining of the alloy, with specific parameters held constant (tool feed rate at 0.4 mm/min, applied voltage at 25 V, and electrolyte concentration at 40 g/liter), results in a notable increase in MRR.

- Conversely, the graphite electrode composed of carbon requires lower temperatures for electron emission and doesn't require an extended timeframe to establish the essential energy pathway to improve the MRR.

- The ANOVA findings for MRR distinctly indicate that the most prominent factor influencing MRR is the electrode type (47.08%), followed by the tool feed rate and other parameters.

- It has been established that the ideal parameter combination for attaining the best SR is TF1-AV1-EC2-ET2, characterized by a tool feed rate of 0.2 mm/min, an applied voltage of 25 V, an electrolyte concentration of 40 g/liter, and the utilization of a brass electrode.

- ANOVA results for surface roughness, clearly illustrating that the most influential factor affecting SR is the tool feed rate (88.33%), followed by the applied voltage and other related parameters

- Furthermore, it is worth noting that the brass electrode consistently delivers superior surface finishes with minimal tool erosion. The surface examination through scanning electron microscopy (SEM) further confirms this observation, revealing an enhanced surface finish when utilizing the brass tool as compared to graphite.

- MATLAB R2016a was utilized to predict the MRR and SR output responses. The experimental data supplied the crucial input–output information needed for training the neural network. The most effective configuration for the ANN model was identified as a 4–12–2 network structure with 4 nodes in the input layer, 12 nodes in the hidden layer, and 2 nodes in the output layer. When examining

all datasets, which include training, validation, and testing data, the correlation coefficient was calculated to be 0.98003.

## Declarations

**Conflict of interest** The authors confirm that there are no conflicts of interest related to the publication of this manuscript.

## References

1. Agrawal, S., Agrawal, S., Kumar Kasdekar, D.: Optimization of MRR and electrolyte coating thickness of ECM parameters using PCA based GRA. Mater. Today Proc. **5**(9), 18956–18965 (2018). https://doi.org/10.1016/j.matpr.2018.06.246

2. Rajesh, S., Gobikrishnan, U., Krishnarjuna Rao, N., Balamurugan, R., Senthilkumar, K.M., Selvan, T.A., Madhankumar, S.: Electrochemical machining of aluminium 7075 alloy, silicon carbide, and fly ash composites: an experimental investigation of the effects of variables on material removal rate. Mater. Today Proc. **62**, 863–867 (2022). https://doi.org/10.1016/j.matpr.2022.04.054

3. Ramakrishna, M.V.A., Venugopal Rao, S.: Fabrication of ECM and study of its parameters in NaCl electrolyte. Mater. Today Proc. **46**, 934–939 (2021). https://doi.org/10.1016/j.matpr.2021.01.181

4. Ginestra, P., Ferraro, R.M., Zohar-Hauber, K., Abeni, A., Giliani, S., Ceretti, E.: Selective laser melting and electron beam melting of Ti6Al4V for orthopedic applications: a comparative study on the applied building direction. Materials **13**(23), 5584 (2020). https://doi.org/10.3390/ma13235584

5. Lowther, M., Louth, S., Davey, A., Hussain, A., Ginestra, P., Carter, L., Cox, S.: Clinical, industrial, and research perspectives on powder bed fusion additively manufactured metal implants. Addit. Manuf.. Manuf. **28**, 565–584 (2019). https://doi.org/10.1016/j.addma.2019.05.033

6. Demirtas, H., Yilmaz, O., Subasi, L., Gunaydin, A., Bilgin, G.M., Orhangul, A., Nesli, S.: Surface quality improvement using electro chemical machining process for γ-TiAl parts produced by electron beam melting. Procedia CIRP **102**, 240–245 (2021). https://doi.org/10.1016/j.procir.2021.09.041

7. Om Prakash, S., Jeyakumar, M., Sanjay Gandhi, B.: Parametric optimization on electro chemical machining process using PSO algorithm. Mater. Today Proc **62**, 2332–2338 (2022). https://doi.org/10.1016/j.matpr.2022.04.141

8. Selvan, T.A., SivaramKotha, M.N.V.S.A., SwamyChinamilli, N.V.S., Guru Dattatreya, G.S., Rajesh, S., Akshey, P.B., Madhankumar, S.: Taguchi-based grey relational study for multiple criterion optimization on process variables for micro electrochemical machining of inconel super-alloy. Mater. Today Proc. **62**, 882–888 (2022). https://doi.org/10.1016/j.matpr.2022.04.060

9. Biswas, S., Paul, A.R., Dhar, A.R., Singh, Y., Mukherjee, M.: Multi-material modeling for wire electro-discharge machining of Ni-based superalloys using hybrid neural network and stochastic optimization techniques. CIRP J. Manuf. Sci. Technol. **41**, 350–364 (2023). https://doi.org/10.1016/j.cirpj.2022.12.005

10. Patnaik, P.K., Mishra, S.K., Swain, P.T.R., Purohit, A., Parija, S.K., Panda, S.S.: Multi-objective optimization and experimental analysis of electro-discharge machining parameters via Gray-Taguchi, TOPSIS-Taguchi and PSI-Taguchi methods. Mater. Today Proc. **62**, 6189–6198 (2022). https://doi.org/10.1016/j.matpr.2022.05.087

11. Wasif, M., Ahmed Khan, Y., Zulqarnain, A., Amir Iqbal, S.: Analysis and optimization of wire electro-discharge machining process parameters for the efficient cutting of Aluminum 5454 alloy. Alex. Eng. J. **61**(8), 6191–6203 (2022). https://doi.org/10.1016/j.aej.2021.11.048

12. Spedding, T.A., Wang, Z.Q.: Parametric optimization and surface characterization of wire electrical discharge machining process. Precis. Eng. **20**(1), 5–15 (1997). https://doi.org/10.1016/s0141-6359(97)00003-2

13. Huang, J.T., Liao, Y.S.: Optimization of machining parameters of Wire-EDM based on Grey relational and statistical analyses. Int. J. Prod. Res. **41**(8), 1707–1720 (2003). https://doi.org/10.1080/1352816031000074973

14. Rajurkar, K.P., Zhu, D., Wei, B.: Minimization of machining allowance in electrochemical machining. CIRP Ann. Manuf. Technol. **47**(1), 165–168 (1998). https://doi.org/10.1016/s0007-8506(07)62809-1

15. Kozak, J., Rajurkar, K.P., Makkar, Y.: Study of pulse electrochemical micromachining. J. Manuf. Process. **6**(1), 7–14 (2004). https://doi.org/10.1016/s1526-6125(04)70055-9

16. Geethapriyan, T., Kalaichelvan, K., Muthuramalingam, T.: Influence of coated tool electrode on drilling inconel alloy 718 in electrochemical micro machining. Procedia CIRP **46**, 127–130 (2016). https://doi.org/10.1016/j.procir.2016.03.133

17. Tang, L., Li, B., Yang, S., Duan, Q., Kang, B.: The effect of electrolyte current density on the electrochemical machining S-03 material. Int. J. Adv. Manuf. Technol. **71**(9–12), 1825–1833 (2014)

18. Dhobe, S.D., Doloi, B., Bhattacharyya, B.: Analysis of surface characteristics of titanium during ECM. Int. J. Mach. Mach. Mater. **10**(4), 293 (2011)

19. "Notes on Electro Chemical Machining (ECM)." https://mechanicalengineering.blog/electro-chemical-machining-ecm/ (Accessed 06 Sep 2023).

20. Antil, S.K., Antil, P., Singh, S., Kumar, A., Pruncu, C.I.: Artificial neural network and response surface methodology based analysis on solid particle erosion behavior of polymer matrix composites. Materials **13**(6), 1381 (2020). https://doi.org/10.3390/ma13061381

21. Senthilkumar, C., Ganesan, G., Karthikeyan, R.: Study of electrochemical machining characteristics of Al/SiCp composites. Int. J. Adv. Manuf. Technol. **43**(3–4), 256–263 (2009). https://doi.org/10.1007/s00170-008-1704-1

22. Thangamani, G., Thangaraj, M., Moiduddin, K., Mian, S.H., Alkhalefah, H., Umer, U.: Performance analysis of electrochemical micro machining of Titanium (Ti-6Al-4V) alloy under different electrolytes concentrations. Metals **11**(2), 247 (2021). https://doi.org/10.3390/met11020247

23. Mahawish, A., Ibrahim, S.I., Jawad, A.H., Othman, F.M.: Effect of adding silicon carbide and titanium carbide nanoparticles on the performance of the cement pastes. J. Civ. Environ. Eng. **07**(04) (2017)

24. Elmolla, E.S., Chaudhuri, M., Meselhy, M.: The use of artificial neural network (ANN) for modeling of COD removal from antibiotic aqueous solution by the Fenton process. J. Hazard. Mater. **179**(1–3), 127–134 (2010). https://doi.org/10.1016/j.jhazmat.2010.02.068

25. Anderson, M.J.: RSM simplified, optimizing processes using response surface methods for design of experiments, 2nd ed., Productivity Press, New York, 2017. https://doi.org/10.1201/978131 5382326

26. Yetilmezsoy, K., Demirel, S.: Artificial neural network (ANN) approach for modeling of Pb (II) adsorption from aqueous solution by Antep pistachio (*Pistacia Vera* L.) shells. J. Hazard. Mater. **153**(3), 1288–1300 (2008). https://doi.org/10.1016/j.jhaz mat.2007.09.092

27. Gugulothu, B., Karumuri, S., Vijayakumar, S., Muthuvel, B., Seetharaman, S., Jeyakrishnan, S., Saxena, K.K.: Optimization of TIG welding process parameters on chrome alloy steel using Box–Behnken method. Int. J. Interact. Des. Manuf. (IJIDeM) (2023). https://doi.org/10.1007/s12008-023-01531-1

28. Karumuri, S., Haldar, B., Pradeep, A., Karanam, S.A.K., Sri, M.N.S., Anusha, P., Vijayakumar, S.: Multi-objective optimization using Taguchi based grey relational analysis in friction stir welding for dissimilar aluminium alloy. Int. J. Interact. Des. Manuf. (IJIDeM) (2023). https://doi.org/10.1007/s12008-023-01529-9

29. Rajesh, M., Sri M.N.S., Jeyakrishnan, S., Anusha, P., Manikanta, J.E., Sateesh, N. et al.: Optimization parameters for electro discharge machining on Nimonic 80A alloy using grey relational analysis. Int. J. Interact. Des. Manuf. (IJIDeM). 2023.

30. Rufina, R.D.J., Uthayakumar, H., Thangavelu, P.: Prediction of the size of green synthesized silver nanoparticles using RSM-ANN-LM hybrid modeling approach. Chem. Phys. Impact **6**(100231), 100231 (2023). https://doi.org/10.1016/j.chphi.2023.100231

31. Plumb, A.P., Rowe, R.C., York, P., Brown, M.: Optimisation of the predictive ability of artificial neural network (ANN) models: a comparison of three ANN programs and four classes of training algorithm. Eur. J. Pharm. Sci. **25**(4–5), 395–405 (2005). https://doi.org/10.1016/j.ejps.2005.04.010

32. Nanda, S.K., Tripathy, D.P., Nayak, S.K., Mohapatra, S.: Prediction of rainfall in india using artificial neural network (ANN) models. Int. J. Intell. Syst.Intell. Syst. **5**(12), 1 (2013). https://doi.org/10.5815/ijisa.2013.12.01

33. Gugulothu, B., Saminathan, R., Pradeep, A., Sharma, A., Vijayakumar, S., Paramasivam, P., Srinivasa Rao, N.: Investigating the strength of butt-welded joints of AA6082 and AA5052 alloys through friction stir welding; the impact of tool tilt angle and feed rate. J. Adhes. Sci. Technol.Adhes. Sci. Technol. (2023). https://doi.org/10.1080/01694243.2023.2253631

34. Anusha, P., Sri, M.N.S., Vijayakumar, S., Rao, T.V.J., Paramasivam, P., Jeyakrishnan, S., Saxena, K.K.: Design and optimization the wear characteristics for Al7178/TiO2/B4C/FA central hybrid composite. Int. J. Interact. Des. Manuf. (IJIDeM) (2023). https://doi.org/10.1007/s12008-023-01341-5

35. Gugulothu, B., Bharadwaja, K., Vijayakumar, S., Rao, T.V.J., Sri, M.N.S., Anusha, P., Agrawal, M.K.: Modeling and parametric optimization of electrical discharge machining on casted composite using central composite design. Int. J. Interact. Des. Manuf. (IJIDeM) (2023). https://doi.org/10.1007/s12008-023-01323-7

36. Boopathy, G., Vanitha, V., Karthiga, K., Gugulothu, B., Pradeep, A., Pydi, H.P., Vijayakumar, S.: Optimization of tensile and impact strength for injection moulded nylon 66/SiC/B4c composites. J. Nanomater.Nanomater. **2022**, 1–9 (2022). https://doi.org/10.1155/2022/4920774

37. Pydi, H.P., Pasupulla, A.P., Vijayakumar, S., Indira, K.P.: Defect analysis and evaluation of mechanical properties of tig welded chrome alloy steel joints for high temperature applications. In: AIP conference proceedings (2022)

38. Manickam, S., Pradeep, A., Vijayakumar, S., Mosisa, E.: Optimization of arc welding process parameters for joining dissimilar metals. Mater. Today Proc. (2022). https://doi.org/10.1016/j.matpr.2022.06.548

39. Pradeep, A., Kavitha, N., Janardhana Rao, T.V., Vijayakumar, S.: Influence of nano alumina/vegetable oil based cutting fluid on MQL turning of stainless steel 304. Mater. Today Proc. (2022). https://doi.org/10.1016/j.matpr.2022.06.547

40. Pydi, H.P., Pasupulla, A.P., Vijayakumar, S., Agisho, H.A.: Study on microstructure, behavior and Al2O3 content flux A-TIG weldment of SS-316L steel. Mater. Today Proc. **51**, 728–734 (2022). https://doi.org/10.1016/j.matpr.2021.06.218

41. Gugulothu, B., Nagarajan, N., Pradeep, A., Saravanan, G., Vijayakumar, S., Rao, J.: Analysis of mechanical properties for Al-MMC fabricated through an optimized stir casting process. J. Nanomater.Nanomater. **2022**, 1–7 (2022). https://doi.org/10.1155/2022/2081189

42. Pal, D., Vijayakumar, S., Rao, T.V.J., Babu, R.S.R.: An examination of the tensile strength, hardness and SEM analysis of Al 5456 alloy by addition of different percentage of SiC/flyash. Mater. Today Proc. (2022). https://doi.org/10.1016/j.matpr.2022.02.288

43. Sharma, P., Paramasivam, P., Bora, B.J., Sivasundar, V.: Application of nanomaterials for emission reduction from diesel engines powered with waste cooking oil biodiesel. Int. J. Low-Carbon Technol. **18**, 795–801 (2023). https://doi.org/10.1093/ijlct/ctad060

44. Bas, D., Dudak, F.C., Boyacı, I.H.: Modeling and optimization III: reaction rate estimation using artificial neural network (ANN) without a kinetic model. J. Food Eng. **79**(2), 622–628 (2007). https://doi.org/10.1016/j.jfoodeng.2006.02.021

45. Vijayakumar, S., Arunkumar, A., Pradeep, A., Satishkumar, P., Singh, B., Rama Raju, K.S., Sharma, V.K.: Optimization of process variables for shielded metal arc welding dissimilar mild steel and medium carbon steel joints. J. Adhes. Sci. Technol.Adhes. Sci. Technol. (2023). https://doi.org/10.1080/01694243.2023.2227461

46. Dombaycı, Ö.A., Gölcü, M.: Daily means ambient temperature prediction using artificial neural network method: a case study of Turkey. Renew. Energy **34**(4), 1158–1161 (2009). https://doi.org/10.1016/j.renene.2008.07.007

47. Vijayakumar, S., Anitha, S., Arivazhagan, R., Hailu, A.D., Rao, T.V.J., Pydi, H.P.: Wear investigation of aluminum alloy surface layers fabricated through friction stir welding method. Adv. Mater. Sci. Eng. **2022**, 1–8 (2022). https://doi.org/10.1155/2022/4120145

48. Nasr, M.S., Moustafa, M.A.E., Seif, H.A.E., El, G.: Kobrosy, application of artificial neural network (ANN) for the prediction of EL-AGAMY wastewater treatment. Alex. Eng. J. **51**(1), 37–43 (2012). https://doi.org/10.1016/j.aej.2012.07.005

49. Somasundaram, M., Saravanathamizhan, R., Basha, C.A., Nandakumar, V., Begum, S.N., Kannadasan, T.: Recovery of copper from scrap printed circuit board: modelling and optimization using response surface methodology. Powder Technol. **266**, 1–6 (2014). https://doi.org/10.1016/j.powtec.2014.06.006

50. Sapkal, R.T., Shinde, S.S., Mahadik, M.A., Mohite, V.S., Waghmode, T.R., Govindwar, S.P., Rajpure, K.Y., Bhosale, C.H.: Photoelectrocatalytic decolorization and degradation of textile effluent using ZnO thin films. J. Photochem. Photobiol. B Biol. **114**, 102–107 (2012). https://doi.org/10.1016/j.jphotobiol.2012.05.016

51. Paramasivam, P., Vijayakumar, S.: Mechanical characterization of aluminium alloy 6063 using destructive and non-destructive testing. Mater. Today Proc. (2021). https://doi.org/10.1016/j.matpr.2021.04.312

52. Gugulothu, B., Satheesh Kumar, P.S., Srinivas, B., Ramakrishna, A., Vijayakumar, S.: Investigating the material removal rate parameters in ECM for Al 5086 alloy-reinforced silicon carbide/flyash hybrid composites by using Minitab-18. Adv. Mater. Sci. Eng. **2021**, 1–6 (2021). https://doi.org/10.1155/2021/2079811

53. Rani, P., Mishra, R.S., Mehdi, H.: Effect of nano-sized Al2O3 particles on microstructure and cmechanical properties of aluminum matrix composite fabricated by multipass FSW. Part C J. Mech. Eng. Sci. (SAGE) (2022). https://doi.org/10.1177/095440622211 10822

54. Mehdi, H., Mehmood, A., Chinchkar, A., Hashmi, A.W., Malla, C., Mohapatra, P.: Optimization of process parameters on the mechanical properties of AA6061/Al$_2$O$_3$ nanocomposites fabricated by multi-pass friction stir processing. Mater. Today Proc. **56**(4), 1995–2003 (2021). https://doi.org/10.1016/j.matpr.2021.11.333

55. Jain, S., Mishra, R.S., Mehdi, H.: Influence of SiC microparticles and multi-pass FSW on weld quality of the AA6082 and AA5083 dissimilar joints. SILICON (2023). https://doi.org/10.1007/s12633-023-02455-x

56. Hashmi, A.W., Mehdi, H., Mishra, R.S., Mohapatra, P., Kant, N., Kumar, R.: Mechanical properties and microstructure evolution of AA6082/Sic nanocomposite processed by multi-pass FSP. Trans. Indian Inst. Met. **75**, 2077–2090 (2022). https://doi.org/10.1007/s12666-022-02582-w

57. Mehdi, H., Mishra, R.S.: Consequence of reinforced SiC particles on microstructural and mechanical properties of AA6061 surface composites by multi-pass FSP. J. Adhes. Sci. Technol.Adhes. Sci. Technol. **36**(12), 1279–1298 (2022). https://doi.org/10.1080/01694243.2021.1964846

58. Mehdi, H., Mishra, R.S.: Effect of multi-pass friction stir processing and SiC nanoparticles on microstructure and mechanical properties of AA6082-T6. Adv. Ind. Manuf. Eng. **3**, 100062 (2021). https://doi.org/10.1016/j.aime.2021.100062